Research Paper

Multidisciplinary design and manufacturing of a Tesla pump prototype

A. Bakogianni [a], E.P. Anselmi [a], D.J. Rajendran [a], L. Bufalari [b], L. Talluri [b], P. Ungar [b], D. Fiaschi [b,*]

[a] Cranfield University, Centre for Propulsion and Thermal Engineering, Bedford MK43 0AL, UK
[b] Department of Industrial Engineering, University of Florence, Via S. Marta 3, Italy

ARTICLE INFO

ABSTRACT

To widen the range of hydraulic efficiencies of boundary layer pumps, a full design methodology has been proposed in order to identify critical issues for their performance and manufacturing. The methodology integrated a 2D numerical code, CFD and FEM analyses, coupled with manufacturing assessments as feedback mechanism. Considering budget constraints and in-house machining capabilities, a quick first prototype was produced. Analyses of the design are pointing out that the volute design initially chosen will not help to achieve an increase in the overall efficiency. The curves of head achieved with 2D and CFD are in agreement, but the latter determines the losses with larger accuracy, thus achieving lower values of head. The 2D model shows limits in the determination of the efficiency, effectively corrected by the CFD analysis. Critical parameters as disc thickness and gap between discs will require a more sophisticated assembly process and materials outsource. The proposed methodology could be used as a reference for the design and performance evaluation of this kind of turbomachinery in the future. The procedure lead to a prototype design, whose optimal efficiency slightly lower than 30 % was achieved at 5000 rpm with 0.3 mm disks gap.

1. Introduction

Current and past studies about Boundary layer pumps have not yet demonstrated how to overcome low hydraulic efficiencies compared with other type of pumps. Furthermore, published theoretical and experimental results differ broadly about the range of overall expected efficiencies. These facts have discouraged the use of boundary layer pumps in stablished industry applications. Interestingly, those who had investigated these mechanisms intensively in the 60 and 70's, Rice [1], Hasinger & Kehrt [2], Balje [3] and Morris [4] to name a few, always stressed the inherent appeal of a pumping device with low susceptibility to cavitation. This characteristic left the door open for applications dealing with small flows of exotic fluids (density and viscosity well apart from water) or requiring small cavitation heads and very high rotational speed. However, future power plants, thermal management and poly-energy generation systems are requiring all these features plus an increased overall efficiency to consider boundary layers a relevant alternative.

Boundary layer pumps, also known as Tesla pumps, friction pumps or shear-force pumps, are made of smooth, numerous small spaced co-axial parallel discs keyed on a drive shaft. This assembly represents the rotor of the pump, which is placed inside a casing with small radial and axial clearance. The fluid is fed to the pump rotor through holes or slots near the shaft and leaves the pump through a volute/diffuser located in the pump casing. In this bladeless device, the pumping does not impinge on the rotating pump mechanism, thus generating a pulsation-free, laminar flow pattern through the pump [5]. As its name indicates, the mechanism was invented by Nikola Tesla, who first applied for the patent in 1909 based on his ideas of converting mechanical rotation into fluid flow energy, and later in 1911 for the turbine (opposite scenario), and both were accepted by the US Patent Office in 1913 [6]. After its invention and for several decades, the Tesla boundary layer turbomachinery remained mainly a conceptual design, due to the low efficiency compared to traditional bladed turbomachinery, which dominated the run towards centralized powerplants and industrialization. In the 50 and 60s of 20th century, there was a revamped interest towards the boundary flow turbomachinery and several studies were carried out to get deeper insights on the flow characteristics between rotating discs [2,7–15]. In 1960, Hasinger and Kehrt [2] investigated analytically and experimentally a Tesla pump using water as working fluid. Instead of flat discs, slightly conical discs were used to increased stiffness. Combining the results with the mathematical model, the predictions indicated that a

rotor efficiency up to 60 % would be possible. Early works on incompressible laminar flows between rotating discs were presented in 1960s by Rice et al. [10–14]. Rice did experimental investigations of multiple discs rotor. Three different prototypes were designed and tested: a water pump, an air compressor, and an air blower. Particularly relevant was the work of Rice in 1965 [15]. The results were compared with non-dimensional model, in order to provide general rules for modelling a Tesla rotor. In 1980, Morris [4] investigated the influence of the gap spacing using water and water-glycol as working fluids. The investigation provided a broad and detailed set of experimental results, demonstrating that disc pump efficiency did not show a strong dependency on disc's gap but certain effect in the head.

However, the interest towards bladeless turbomachinery dropped again in the 1970s, because of the larger attractiveness of higher efficiency bladed machines, despite the improvements achieved in boundary layer technology in the previous decade. Only few relevant works on Tesla pump were carried out. One of these is the one of Darby in 1987 [16], who presented an experimental evaluation of the performance and characteristic of a water Tesla pump. Multiple configurations were used in this project, in order to obtain and compare different results. In early 2000s, the interest towards Tesla turbomachinery was revamped and currently some applications where the Tesla pump could be useful are available, in compliance with how suggested by Rice in 1965 [11]. Foster [17], in 2006 addressed the usefulness of Tesla in pumping blood because of its working principle, which allows preserving the blood quality when pumped. In 2007, Bloudiček [18] worked on the design, manufacturing and testing of a water Tesla turbine, with the objective of achieving a significant effectiveness. In 2014, Wang [19] designed and built an experimental test rig for a shear force pump. The objective of the paper was investigating the internal flow dynamics and clarifying the loss mechanism. It demonstrated that the rotor performance alone of such machines is comparable with centrifugal machines, being the integration with a volute which causes significant performance losses. In 2015, Dodsworth and Groulx [20] presented a document about the study of a Tesla pump aimed at finding a relationship between discs' gap and efficiency. In 2020, Talluri et al. [21] investigated the optimal design procedure of Tesla turbines for ORC applications. A thorough optimization method was performed by evaluating the losses of each component and by introducing an innovative rotor model. This model could be also used for Tesla pump applications. In 2019, Martinez-Diaz [22] published an article on the effects of turbulization on the pump discs' performance. The objective was increasing the performance of this pump developing a new experimental study based on the turbulization of flow by placing turbulizers into the inter disc channel output. In 2021, Anselmi et al. [23] developed a numerical model to design a Tesla pump using water as working fluid. In 2019, Alonso [24], discussed about possible ways of increasing the efficiency of boundary layer pumps through optimizing the rotor's geometry utilizing slightly curved channels in place of straight ones. In 2020, Heng [25] published a paper about the preliminary experimental work on a novel pump model, specifically designed to transport slurry and multiphase flows. The prototype corresponded to at Tesla pump rotor adapted into an existing commercial centrifugal volute for the offshore petroleum deep-sea application. In 2019, Renuke et al. [26,27] published groundbreaking results after investigating the experimental and numerical performance of Tesla turbines for micro power generation using a flexible test rig with air as the working fluid. Major losses and the effect of design parameters on turbine performance were evaluated, contributing also to research on Tesla pumps.

The literature review showed that a crucial point is that the rotor efficiency in a boundary layer pump is satisfactory but its integration with a volute derives in the low overall efficiency found in experimental tests. Here resides the challenge, how to integrate these two components in a meaningful and systematic approach, increasing the efficiency of the boundary layer at comparable levels with conventional bladed pumps. The answer, not surprisingly, is related with the design
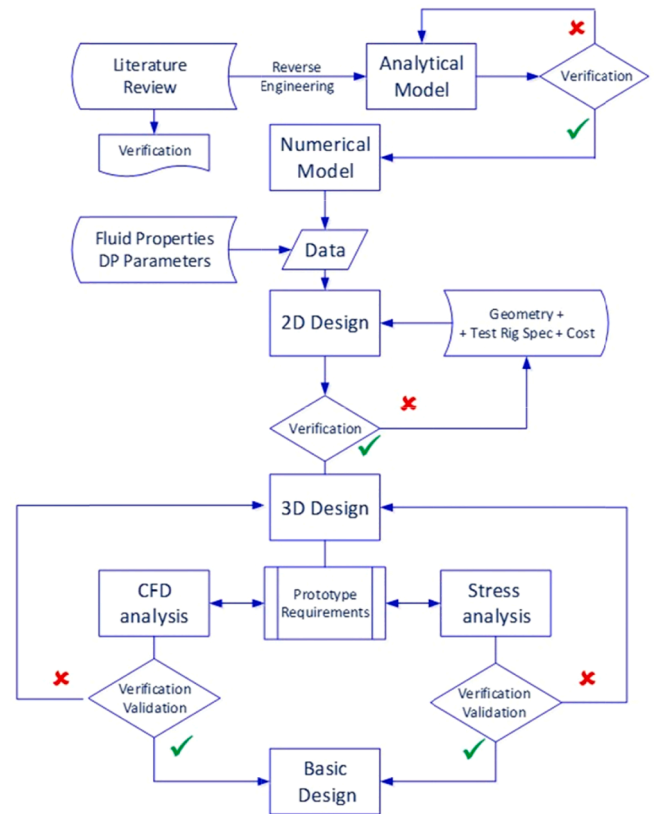

Fig. 1. General design methodology.

methodology followed. This research discusses the first lessons learned after performing independent studies to produce and manufacture a first boundary layer pump prototype. The design and performance assessment of the prototype can be summarised in three fundamental steps:

1) Basic design and geometry definition by using a previously developed 2D model, with validation against experimental data from literature.
2) Design refinement through the CFD applied to rotor and stator, using methods previously exercised for the investigation of published geometries.
3) Mechanical design of the Tesla pump prototype, supported FEM studies with modal analysis and assessment of critical frequencies.

Such a comprehensive design of a Tesla pump is currently not available in literature. For this reason, it may become a reference for the design and performance evaluation of this kind of turbomachinery. At the same time, it paves the way for testing the prototype, which will provide results to verify and validate the numerical models associated.

2. Methodology

The methodology described in this paper reflects current efforts to develop and test a first prototype for a boundary layer pump as a mean to assess future and more complex designs. Following an approach of "learning by doing", studies have been conducted independently but keeping record of assumptions, boundary conditions and interfaces. Fig. 1 shows the general methodology used. Parametric analysis of the prototype performance is included as part of the 2D design.

The Tesla pump prototype was developed with minimal specifications, consisting of a bladeless rotor composed of parallel thin discs fixed to a rotating shaft, a single volute which includes an external casing, and inlet/outlet connections.
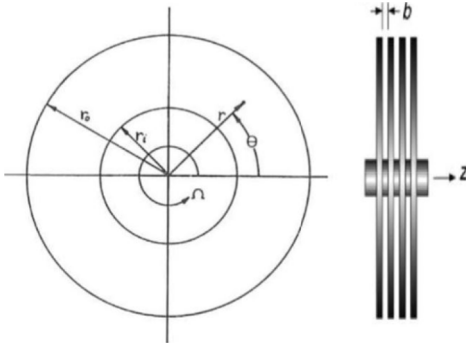
Fig. 2. Schematic of Tesla pump rotor cylindrical coordinates.

2.1. 2D basic rotor and stator modelling

The 2D rotor model is derived from the one developed and validated for ORC Tesla expanders in [21,24,25], readapted to the reverted pumping effect with incompressible water as working fluid [18]. Here it is shortly summarized.

The flow between discs is considered steady, laminar, viscous, and parabolic, with body forces negligible compared to viscous ones. Moreover, a radial and symmetric flow field is considered, uniform at the inlet ($r = r_i$). For this reason, the flow field is invariable with θ, therefore its derivative in tangential direction $\partial/\partial\theta = 0$ for all flow variables. Finally, the flow has no components on z axial direction ($v_z = 0$). With reference to cylindrical coordinates r, θ (Fig. 2), the relative velocities in radial r and tangential θ directions can be expressed as:

$$w_r(r,z) = \overline{w_r}a\frac{z}{b}\left(1-\frac{z}{b}\right) \tag{1}$$

$$w_\theta(r,z) = \overline{w_\theta}a\frac{z}{b}\left(1-\frac{z}{b}\right) \tag{2}$$

$a = 7$ for completely developed flow; $a = 4$ for non-developed flow (inlet region).

The Navier-Stokes equations in cylindrical coordinates follow:

$$\text{Continuity}: \quad \frac{1}{r}\frac{\partial(r\rho w_r)}{\partial r} = 0 \tag{3}$$

$$\text{Momentum, r} - \text{direction}: \quad w_r\frac{\partial w_r}{\partial r} - \Omega^2 r - 2\Omega w_\theta - \frac{w_\theta^2}{r}$$
$$= -\frac{1}{\rho}\frac{\partial p}{\partial r} + \frac{\upsilon\partial^2 w_r}{\partial^2 z} \tag{4}$$

$$\text{Momentum, }\theta - \text{direction}: \quad w_r\frac{\partial w_\theta}{\partial r} + \frac{w_r w_\theta}{r} + 2\Omega w_r = \frac{\upsilon\partial^2 w_\theta}{\partial^2 z} \tag{5}$$

$$\text{Momentum, z} - \text{direction}: \quad \frac{\partial p}{\partial z} = 0 \tag{6}$$

Integrating the differential form of the r and θ momentum equations between $z = 0$ and $z = \frac{b}{2}$, and assuming the maximum velocity value at mid-channel and zero velocity at the walls, the equations of the motion are obtained:

$$\text{r} - \text{direction} \quad \frac{1}{\rho}\frac{dp}{dr} = -\frac{a^2}{30}w_r\frac{\partial w_r}{\partial r} + \Omega^2 r + \frac{a}{6}2\Omega w_\theta + \frac{a^2}{30}\frac{w_\theta^2}{r} - \frac{2a}{b^2}\upsilon w_r \tag{7}$$

$$\theta - \text{direction} \quad \frac{\partial w_\theta}{\partial r} = -\frac{10}{a}\Omega - \left(\frac{60\upsilon}{w_r b^2 a} + \frac{1}{r}\right)w_\theta \tag{8}$$

In (1 – 8), the following nomenclature is used:

- w_r, w_θ: relative radial and tangential velocities
- $\overline{w_r}, \overline{w_\theta}$: relative radial and tangential average velocities
- $\dot{m}_{ch}$: mass flowrate into the channel
- b: discs gap
- ρ: density
- Ω: rotational speed
- p: pressure
- r: radius
- ν: kinematic viscosity

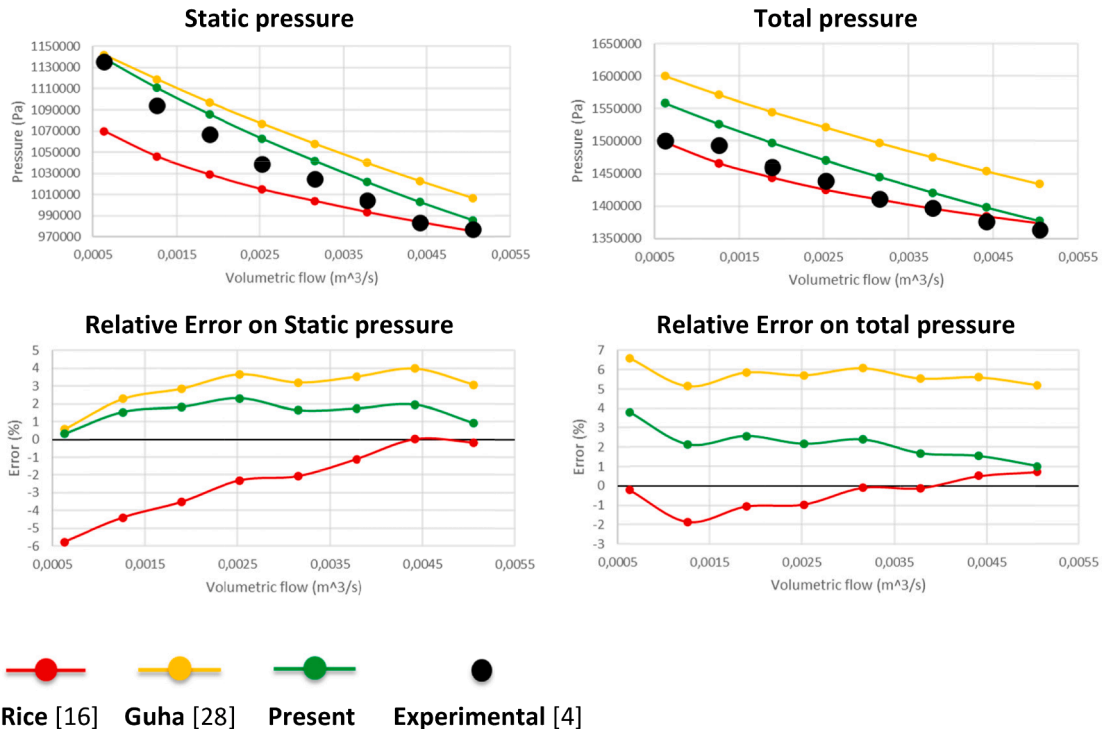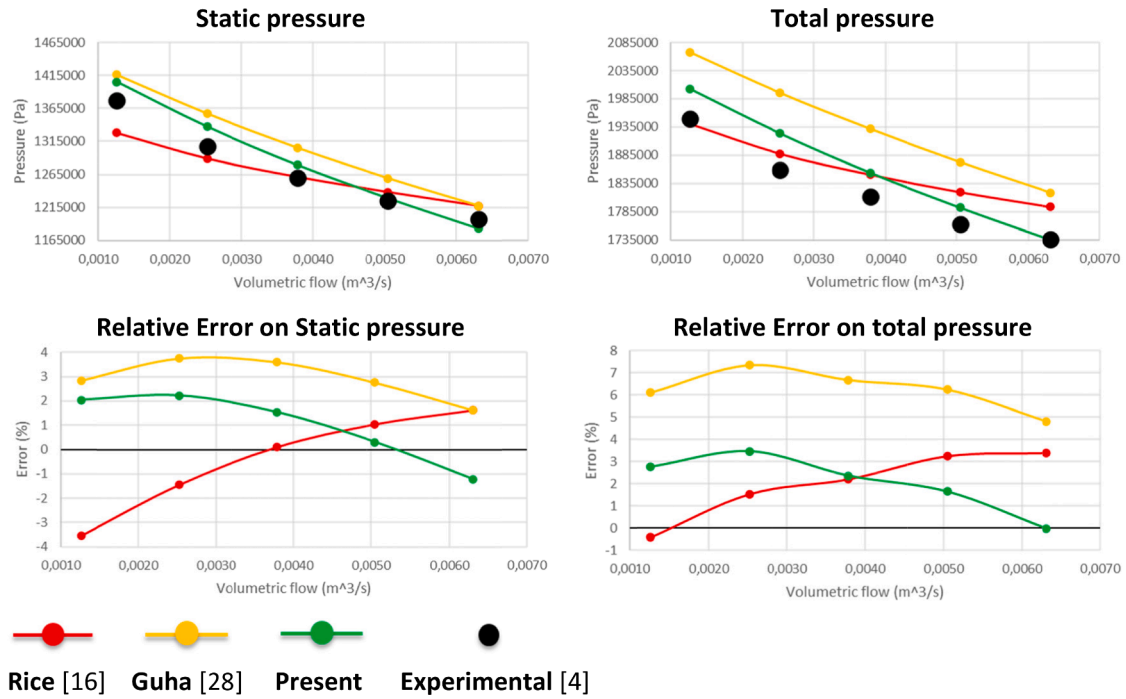**Fig. 3.** Present model results vs experimental and other models results, $\Omega = 5000$ rpm.

Fig. 4. Present model results vs experimental and other models results, $\Omega = 6000$ rpm.

Table 1
Comparison of average errors between different models and experimental data of rotor.

Model	Average error on static pressure [%]	Average error on total pressure [%]
Rice	2	2.05
Guha	3.15	5.7
Present	1.99	2.14

- a: coefficient
- z: axial direction

2.2. Validation of 2D modelling

The validation of the rotor model has been done against the experimental results of Morris [4] and with the numerical model results of Guha [20] and Rice [15]. The parameters used for the comparison between the models and the experimental results are the rotor discharge static and total pressure, p_2 and p_{02} respectively. Among the different conditions evaluated experimentally by Morris [4] the following has been selected: *rotor external diameter:* 5.94 in (150.9 mm)*, rotor internal diameter:* 1.5 in (38.1 mm)*, disk spacing:* 0.006 in (0.15 mm)*, disk thickness:* 0.005 in (0.127 mm)*. Moreover, the following conditions have been imposed at the water inlet section while evaluating the different numerical models, in accordance to Morris's experimental condition: *inlet pressure:* 50 psi$_g$ (4.46 bar$_g$), *inlet temperature:* 55 °C.

The relative error between models results and experimental data is defined as:

$$\text{error } [\%] = \frac{(p_{model} - p_{experimental})}{p_{experimental}} * 100$$

The results of present model verification are summarized in Fig. 3 and Fig. 4, referred to two different rotational speed (e.g. 5000 and 6000 rpm respectively). The agreement of the present model with the experimental results is rather satisfactory compared with the other model. The summary comparison of average errors with experimental results is reported on Table 1.
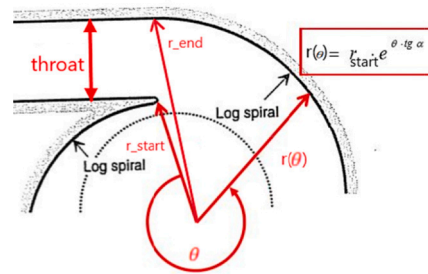

Fig. 5. Schematic of volute geometry and parameters.

The volute model is referred to a logarithmic spiral shaped geometry, shown schematically in Fig. 5 [23].

The following assumptions are adopted in modelling the *intake* and the *volute*:

- Suction losses at intake are negligible.
- Rotor inlet speed is radial.

$$p_1 = p_0 - \rho v_{r1}^2 \tag{9}$$

$$v_{r1} = \frac{\dot{m}}{\rho \pi D_i b} \tag{10}$$

- The volute recovers some of the kinetic energy in terms of pressure.
- The volute collects the outgoing flow from the rotor by conveying it towards the outlet.
- The model of volute considers three different types of losses.
  o Radial velocity dump losses:

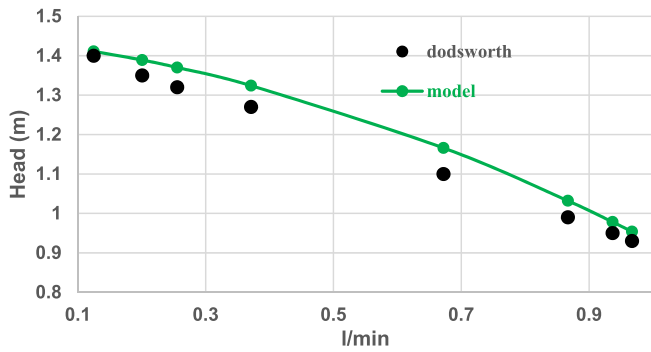$$\Delta p_{sr} = \frac{\rho v_{r2}^2}{2} \tag{11}$$

Fig. 6. Comparison of Tesla characteristic curve from model predictions and experimental data provided in [30].

o Tangential velocity dump losses:

$$\Delta p_{st} = \gamma_t \frac{\rho (v_{t2} - v_{t3})^2}{2} \qquad (12)$$

o Friction losses:

$$\Delta p_a = f \frac{L}{D_h} \rho \frac{\overline{v_t^2}}{2} \qquad (13)$$

where:

- $\overline{v_t}$: average tangential velocity in the volute
- p_1, p_0: inlet rotor and upstream inlet pressures respectively
- v_{r1}, v_{r2}: rotor inlet / outlet absolute radial velocities respectively
- v_{t2}, v_{t3}: volute inlet / outlet absolute tangential velocities respectively
- $\gamma_t = 0.5$ as suggested by Van den Braembussche [29]
- f: friction factor

- L: volute length
- D_h: hydraulic diameter of volute.

The results of the overall Tesla pump model have been verified against the experimental data of Dodsworth's prototype [30]. The outer radius of the volute (e.g. the angle α_v), the inlet and exit pump pipes diameters were not available from the paper, thus they were assumed to run the calculation model at 27.5 mm ($\alpha_v = 3.187°$), 32 mm and 32 mm, respectively. The comparison between the experimental and model predicted characteristic curves is shown on Fig. 6. Considering the uncertainties related to the above-mentioned missing data, the agreement is satisfactory, with maximum and average difference between model and test results at 8.3 % and 4.2 % respectively. Generally, the agreement with experimental data is higher at the lower and higher flowrates, lower at intermediate flowrates.

3. Prototype design

The basic design of the Tesla pump prototype has been carried out with the above discussed 2D thermodynamic model. The main data are selected in compliance with the constraints related to the manufacturing analysis (see also section 6) and summarised in the following:

- Maximum flow rate: 2.3 l/s
- Maximum supply pressure: 220 kPa
- Maximum number of revolutions per minute: 5,000 rpm
- Maximum power supplied by motor: 3,000 W
- Outer diameter of discs: 76 mm
- Disc thickness: 1.2 mm
- Maximum number of discs: 25
- Material: aluminium
- Rotor configurable with different numbers of discs and distance between them.
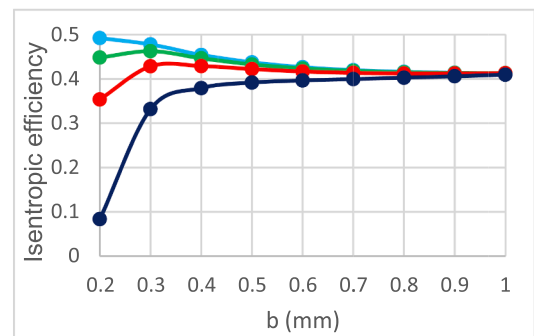
The basic design has been done with thermodynamic optimization of
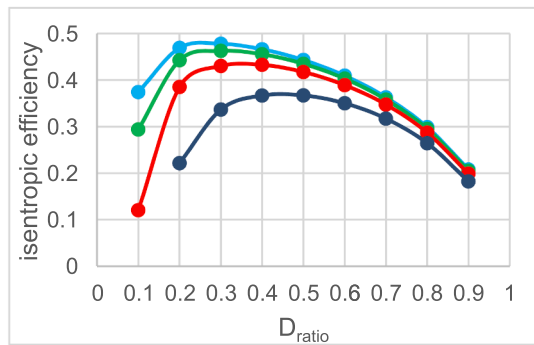
a) rotor isentropic efficiency vs. D_{ratio}
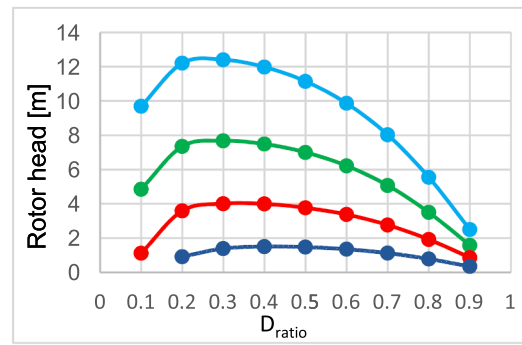
b) head across rotor vs. D_{ratio}

c) rotor isentropic efficiency vs discs gap b

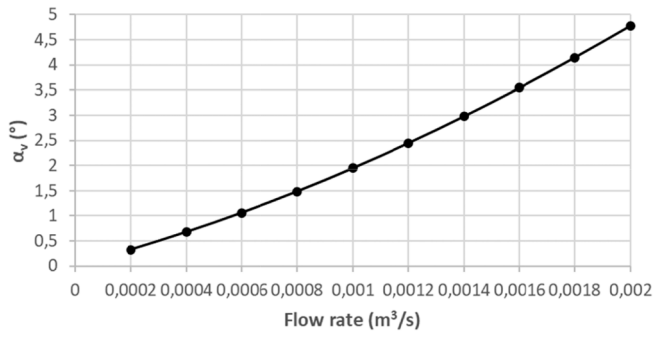**Fig. 7.** Behaviour of Tesla pump rotor performance parameters vs Dratio and discs gap b at variable rotational speed.

Fig. 8. Behaviour of αv vs flowrate at 5000 rpm rotor speed.

the performance data of the rotor and volute. In particular, the two most relevant rotor design parameters are the inner to outer diameter ratio D_{ratio} and the discs gap b. Fig. 7 shows the behaviour of rotor isentropic efficiency (a) and pressure ratio (b) vs D_{ratio} and isentropic efficiency vs discs gap (b) at variable rotational speed and flowrate fixed at 2 l/s.

The rotor isentropic efficiency is defined as:

$$\eta_{rs} = \frac{h_{02s} - h_{01}}{W_r} \tag{14}$$

Where:

h_{02s}: rotor outlet total isentropic enthalpy;
h_{02s}: rotor inlet total enthalpy;
W_r: work of rotor single channel, from Euler's equation $W_r = \omega (r_2 v_{t2} - r_1 v_{t1})$;
ω = rotational speed [rad/s]; r_1 = rotor inner radius; r_2 = rotor outer radius; v_{t1} = rotor inner tangential velocity; v_{t2} = rotor outer tangential velocity.

As it is clear from the figure, the performance parameters are opti-

mized at $D_{ratio} = 0.3$ and b = 0.3 mm. The basic design of the volute is done with the following assumptions:

- Free vortex theory;
- Viscous losses are neglected;
- Conservation of momentum and flow rate along the logarithmic spiral shape of the volute:

$$r_\theta = r_{start} \cdot e^{\theta \cdot tg(\alpha v)}, \ r_\theta(0) = r_{start}; r_\theta(2\pi) = r_{end} \tag{15}$$

- The model takes into account the three different types of losses reported on eqns (11–13) [29].

The friction coefficient f for smooth pipes can be calculate by the Blasius equation:

$$f = 0.3164 Re^{0.25} \tag{16}$$

The value of $\gamma_t = 0.5$, as suggested on [29].
The volute channel length L is given by:

$$L = \left(\frac{r_{end}}{tan(\alpha_v)} - \frac{r_{start}}{tan(\alpha_v)} \right) \sqrt{1 + \tan^2(\alpha_v)} \tag{17}$$

The losses are minimized for an angle α_v related to the flow out of the rotor expressed as:

$$\tan(\alpha_v) = v_{r2}/v_{t2} \tag{18}$$

with v_{r2} and v_{t2} are, respectively, the radial and tangential velocities at rotor outlet. Since the flow exits mainly tangential from the rotor, the required values of α_v are very small. As an example, Fig. 8 shows the behaviour of α_v vs flowrate at 5,000 rpm rotor speed. In the present case, the following volute design parameters are found:
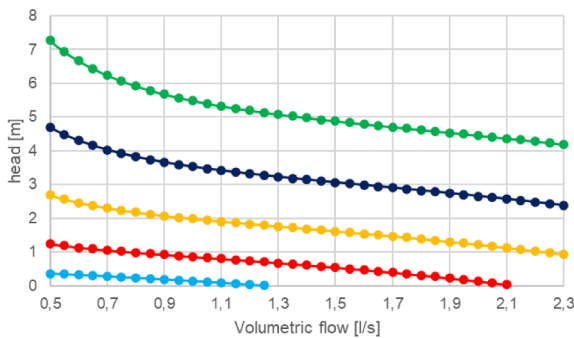
- $\alpha_v = 2.365°$, in order to have a good value for a wide range of volumetric flow rate;
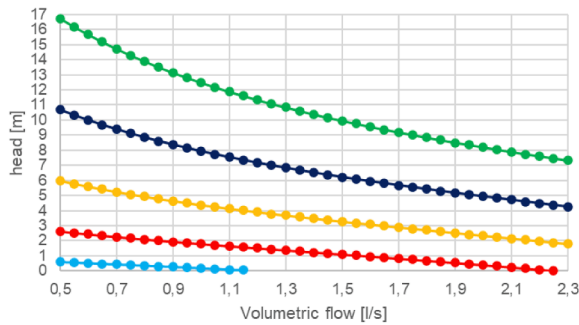
a) b=0.3mm; 25 discs
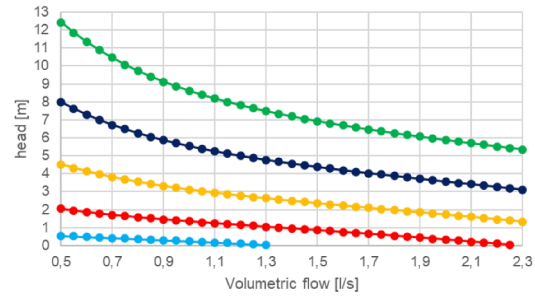
b) b=0.5 mm; 21 discs

c) b=1 mm; 16 discs

Fig. 9. Tesla pump prototype head characteristic curves at variable speed for different discs gap b and number of discs.

a) b=0.3mm; 25 discs
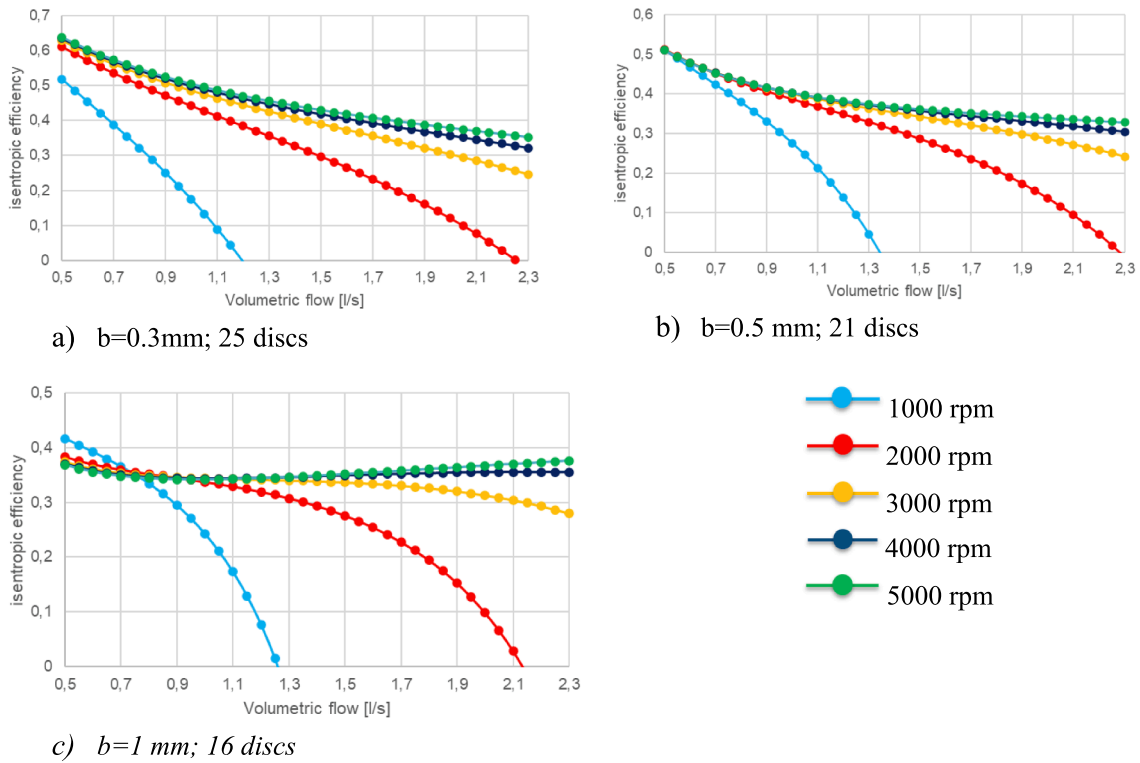
b) b=0.5 mm; 21 discs

c) b=1 mm; 16 discs

Fig. 10. Tesla pump prototype total to total isentropic efficiency characteristic curves at variable speed for different discs gap b and number of discs.

- Minimum gap between the rotor discs and the volute casing = 1 mm;
- Initial volute radius = 39 mm, from eqn (14) at θ = 0;
- End volute radius = 52.5 mm;
- Volute width = 37.8 mm.

3.1. Prototype characteristic curves

Following the proposed described Tesla pump model and in agreement with the above prototype design parameters, the characteristic curves of the designed machine can be derived. Because of the large modularity of the pump, the characteristic curves are reported for different numbers of rotor discs and discs gap b. The curves of head are
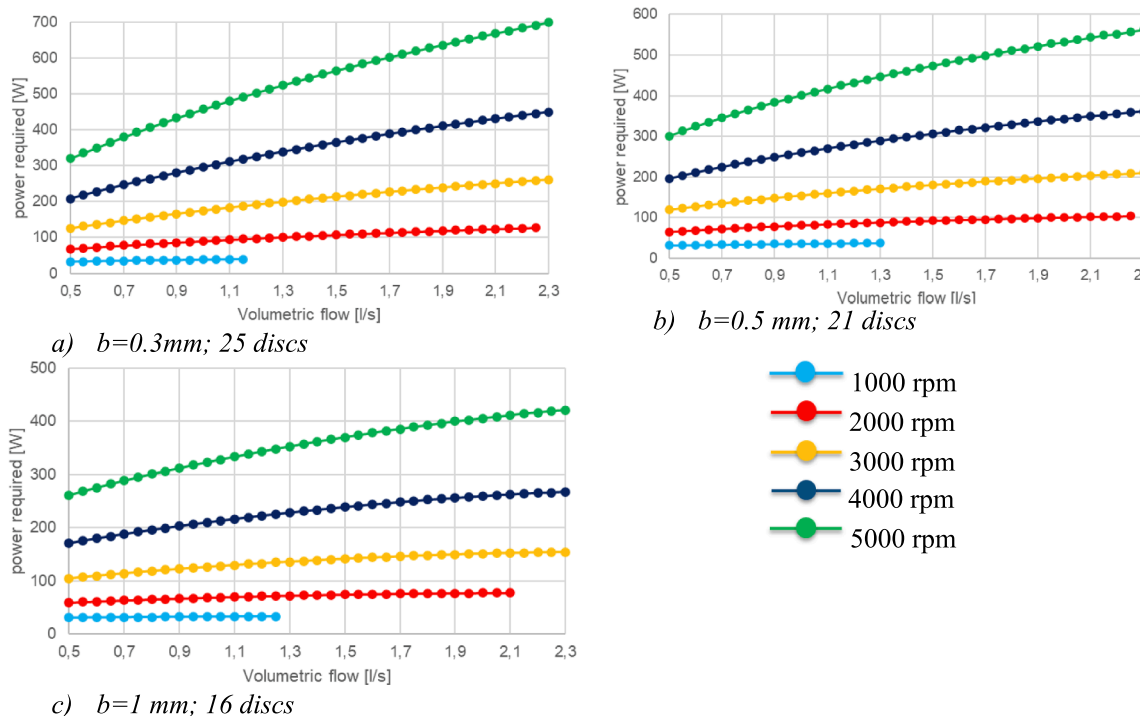

a) b=0.3mm; 25 discs

b) b=0.5 mm; 21 discs

c) b=1 mm; 16 discs

Fig. 11. Tesla pump prototype input power characteristic curves at variable speed for different discs gap b and number of discs.
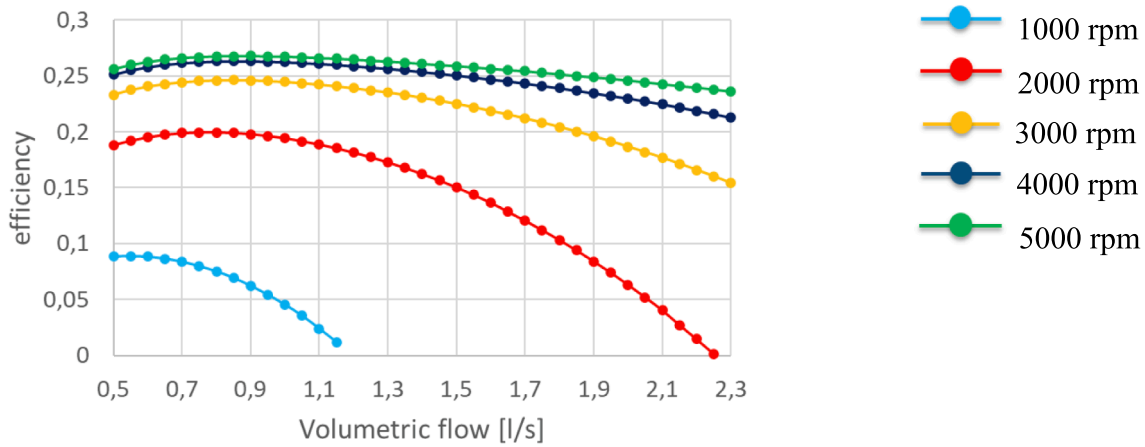
Fig. 12. Tesla pump prototype conventional efficiency characteristic curves at variable speed for different discs gap b and number of discs.

shown on Fig. 9, at three different values of b and disc number.

The pump head, referred to pump output exit pipe (downstream the volute) / rotor input and to static pressures, is defined as:

$$head = \frac{p_{out}}{\rho_{out} \bullet g} + \frac{v_{out}^2}{2 \bullet g} - \left(\frac{p_{in}}{\rho_{in} \bullet g} + \frac{v_{in}^2}{2 \bullet g} \right) \qquad (19)$$

where:

p_{in}, p_{out} = pump inlet (rotor) and outlet (exit pipe) static pressures respectively;

v_{in}, v_{out} = pump inlet (rotor) and outlet (exit pipe) flow velocities respectively;

ρ_{in}, ρ_{out} = pump inlet (rotor) and outlet (exit pipe) flow densities respectively.

As can be observed, the head is reduced with lowering number of discs. Decreasing number of discs and increasing gap, both have the same effect on head. Less discs means less energy given to the fluid and wider gap means less effective shear force at the centre of the gap. It confirms the easy design modularity of the Tesla pump, which target performance may be tuned with variable number of discs. In the three analysed cases of Fig. 9, the gap and number of discs were changed to keep the same volute, as the total widths of the 3 versions a), b) and c) are 37.8 mm, 36.2 mm and 36.2 mm respectively. In the different configurations, the behaviour of the characteristic curves is similar. It differs from that of other pump technologies, like centrifugal ones, which typically exhibit bottom concavity curve. The curves of Tesla pumps approach a linear behaviour at low rpm. This behaviour is reasonable for boundary layer pumps, as also reported in Pacello and Hanas, 2000 [5] and Dodsworth [30].

The maximum 16.7 m head is achieved at 5000 rpm for channels gap b = 0.3 mm. The characteristic curves of isentropic efficiency at the same variable disc gap, number of discs and rotational speed are reported on Fig. 10. The efficiency is generally reduced at lower number of discs. The behaviour tends to be similar with increasing number of discs. At higher rotational speeds, the configurations with lower number of discs show intermediate values of flowrate, slightly minimizing the efficiency. It can be correlated to a maximum value of kinetic energy at the rotor output, leading to a worse conversion of the fluid energy content. It only happens at the larger discs gap. At the other values, the kinetic energy doesn't reach a maximum, but it increases in the whole analysed range of flow rate. It is related to the ratio between flow rate and channel section area which, at low flow rate, leads to a lower efficiency. The highest achieved isentropic efficiency is 63.8 % at 5000 rpm with 0.3 mm channel width.

The power characteristic curves of the designed prototype at variable

Table 2
Tesla pump geometrical characteristics and design parameters.

Parameter	Symbol	Value	Unit
Rotor inlet diameter	D_{in}	25.4	[mm]
Rotor outlet diameter	D_{out}	76	[mm]
Inter-disc gap	b	0.3	[mm]
Disc thickness	t	1.2	[mm]
Volute base circle diameter	Dvol	78	[mm]
Volute spiral angle	α_v	2.365	[deg]
Max volute outlet radius	r_{max}	52.5	[mm]
Volute width	d	37.8	[mm]
Rotor-volute clearance	c	1	[mm]
Number of discs	n	25	[–]
Max supplied power	P	3000	[W]
Max rotational speed	N_{max}	5000	[rpm]
Max flowrate	V_{max}	2.3	[l/s]
Design Point			
Inlet Total Pressure (Abs)	P_{in}	101,325	[Pa]
Inlet Total Temperature	T_{in}	298.15	[K]
Volume Flowrate	V	0.9	[l/s]
Rotational speed	N	5000	[rpm]

discs gap, number of discs and rotational speed are reported on. The power required by the pump is calculated multiplying the torque input to the rotor by its rotational speed., also considering the friction power losses due to seals. The maximum required power is at 699.2 W, obtained at 5000 rpm with channel width at 0.3 mm.

To obtain a conventional value of the efficiency comparable with other Tesla pump studies, the power absorbed by the pump shown in Fig. 11 is set equal to the power required by the pump motor. In this way, the efficiency of the pump is calculated as:

$$\eta = \frac{\dot{m}Hg}{W} \qquad (20)$$

Where $\dot{m}$ = mass flowrate; H = head; g = gravity acceleration; W = shaft input power. The efficiency characteristic curves of the prototype with 25 rotor discs 0.3 mm spaced are shown on Fig. 12. The maximum overall pump efficiency is at 26.8 % level, achieved at 5000 rpm and channel width at 0.3 mm. These values are in line with the efficiency values reported in literature for experimental investigations of discs pump (Morris, 1980 [4]) with similar geometry, flowrate, disks spacing and rotational speed levels.

4. CFD analysis

The Tesla pump geometry is assessed with 3D CFD to capture the flow field and losses in more detail and compare the results with the design code. The secondary flow path is omitted at this stage of research
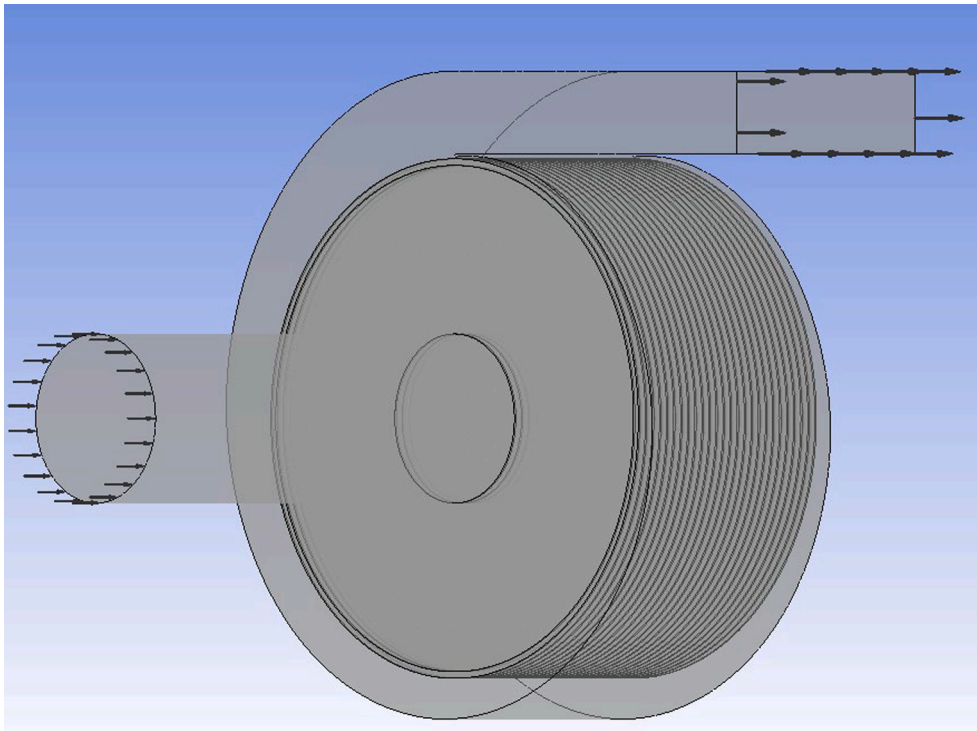
Fig. 13. Image of the full flow domain as it appears in the simulation software.

Table 3
Investigation of axial divisions and their impact on y+ and pump performance parameters.

Axial divisions	Y+	Head [m]	Efficiency [%]
10	40.45	13.14	22.19
30	1.26	13.63	22.87
40	1.14	13.66	22.78

Table 4
Mesh parameters of the three cases and GCI Richardson Extrapolation results.

	Case 1	Case 2	Case 3
Circumferential divisions	200	320	512
Radial divisions	50	80	128
Full model nodes number (millions)	5.27	10.39	23.18

GCI Calculations

	Total Pressure Rise [Pa]	Torque [Nm]
r_{21}	1.6	1.6
r_{32}	1.6	1.6
v_1	122420	1.0017
v_2	123570	0.996
v_3	124220	1.000
P	1.214	0.529
φ_{ext}^{21}	120925	1.021
φ_{ext}^{32}	122725	0.981
e_a^{21}	0.009	0.005
e_{ext}^{21}	0.012	0.019
e_a^{32}	0.005	0.004
GCI_{fine}^{21}	0.015	0.024
GCI_{fine}^{32}	0.009	0.019
Range of convergence [35]	1.009	0.995

since it is not included in the design code. This study focuses on a significant aspect of Tesla pumps that has been reported in literature, the interaction between rotor and volute [31]. The dimensions of the simulated Tesla pump geometry are summarized in Table 2. The geometry is simulated with added pipe-like domains on the inlet and outlet to achieve stability in the inlet and outlet results. from The full fluid domain is shown in Fig. 13. Simulations are run in ANSYS CFX software. The water properties are imported as a table file generated using REFPROP data [32]. The heat transfer model is Total Energy, and the turbulence model is Shear Stress Transport. The boundary conditions of total pressure and temperature are imposed at the inlet and the mass flow at the outlet while the disc walls are rotating. To evaluate the convergence of calculations, the total pressure rise, the shaft torque, the hydraulic efficiency, and the outlet temperature are monitored.

The pipe and volute mesh are tetrahedral, while the rotor mesh is hexahedral. The gap is discretised in the axial direction using inflation layers of growth rate 1.2 on the rotating walls. The number of the axial divisions is investigated focusing on achieving y + values around 1 for better capturing of the boundary layer [33]. This is conducted by an iterative process where the axial divisions of the gap are gradually increased and the average y + at the rotor walls as well as the performance parameters of the fully integrated pump model are evaluated with CFD. The results of y + investigation is shown in Table 3. The radial nodes are always one fourth of the circumferential nodes and the average mesh element size of the pipe and volute domains is taken as equal to the average rotor mesh element size. Thus, the grid independence study is conducted for three cases based on the number of

circumferential divisions of the cylindrical gap with the Richardson extrapolation method [34]. The results are shown in Table 4 below and the final rotor gap mesh (Case 2) is illustrated in Fig. 14.

It is noted that the analysis of the results at the design point is conducted with the 40 axial divisions case for better detail illustration. However, from Table 3 it can be noticed that the overall performance parameters are not significantly affected by the number of axial nodes. Thus, for the generation of the characteristic curves only, 10 axial divisions are considered sufficient and provide computation time efficiency. The pressure contour at a horizontal cross section of the pump in
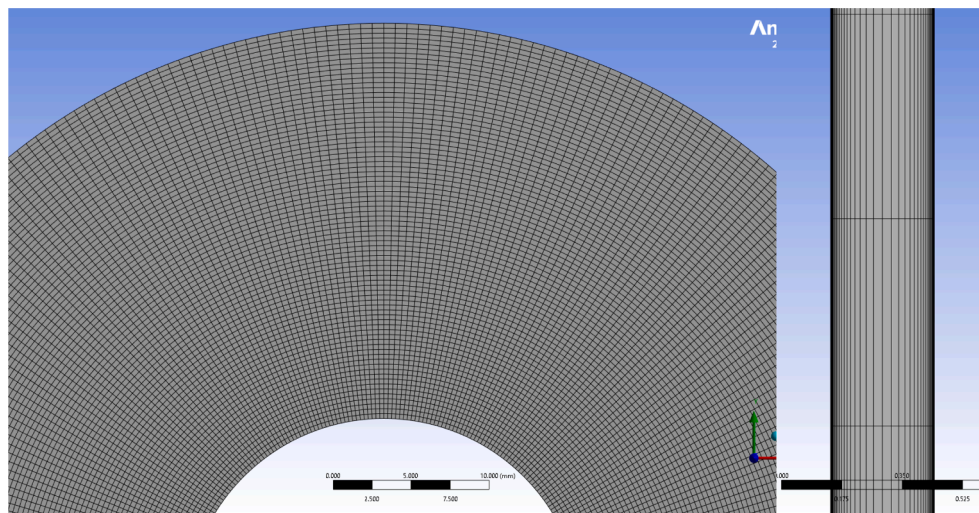
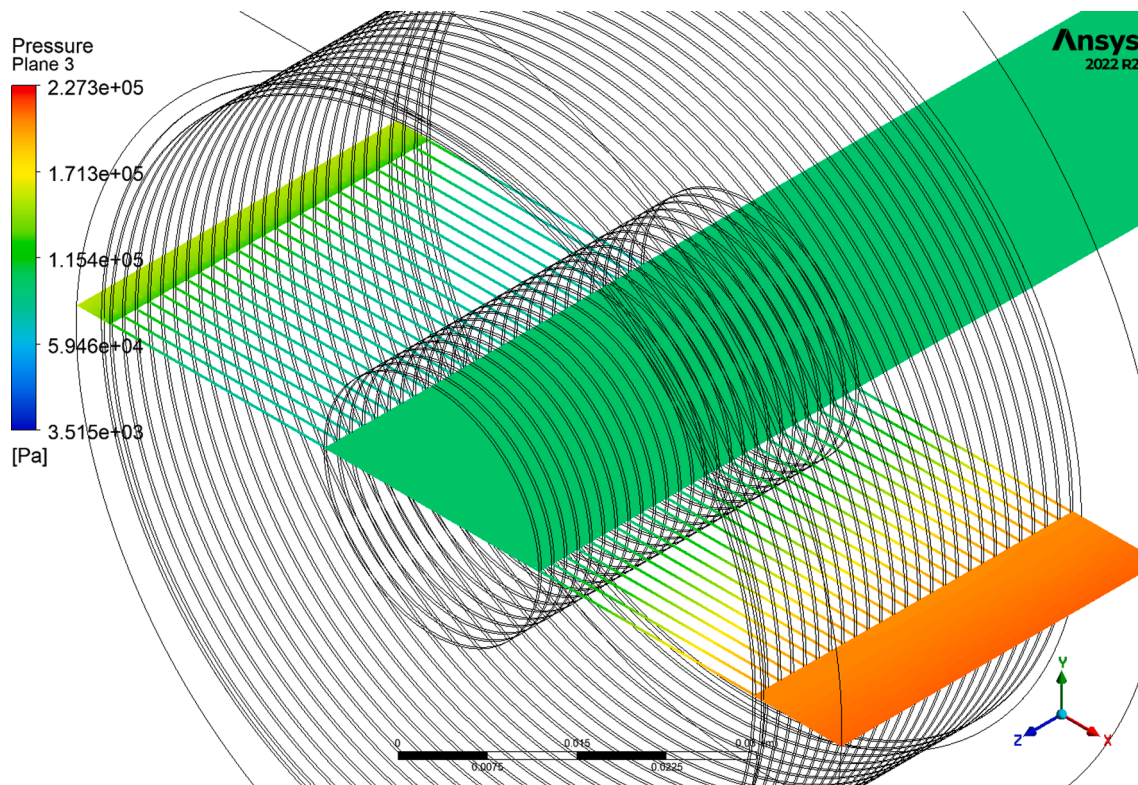**Fig. 14.** Final rotor gap mesh, front and side detail view.

Fig. 15. Pressure contour on an horizontal cross section.

Fig. 15 indicates a smooth pressure increase from the inlet to the outlet and along the volute channel, as expected at every pump.

However, a pressure contour in the middle of a gap shows that the pressure field is very non-axisymmetric, as illustrated in Fig. 16. Further examination of the streamlines (Fig. 17) indicates that there is a flow reversal area, towards the positive direction of x axis, where flow even turns inwards to the inlet instead of being centrifuged towards the outlet. This implies that the volute design is poor in terms of cross-sectional areas and the clearance between the rotor and volute is too small, so the rotor flow is heavily affected. The vector contours compare the positive and the negative x sides of the pump (Figs. 18 and 19), confirming that the flow reversal is obvious. From the streamlines, it seems that at the areas where the angle in which the fluid leaves the

rotor is far from the volute angle deceleration and too high local pressure rise appears in the volute, which pushes the fluid back into the rotor.

In the following Figs. 20 and 21. the pump characteristics and hydraulic efficiencies respectively, as produced by CFD simulations, are compared with the results of the 2D code. The CFD results agree with the 2D code results in terms of the trends of total pressure rise. However, the head appears to be lower in the CFD results because the pressure losses are calculated in a more accurate way. Table 5 illustrates the mean absolute error of the head between the 2D code and the CFD results for every curve, which can be very high especially at the lower rotational speeds. In terms of efficiency, the 2D code results do not match with the CFD ones not only because of the mismatch in total pressure rise, but
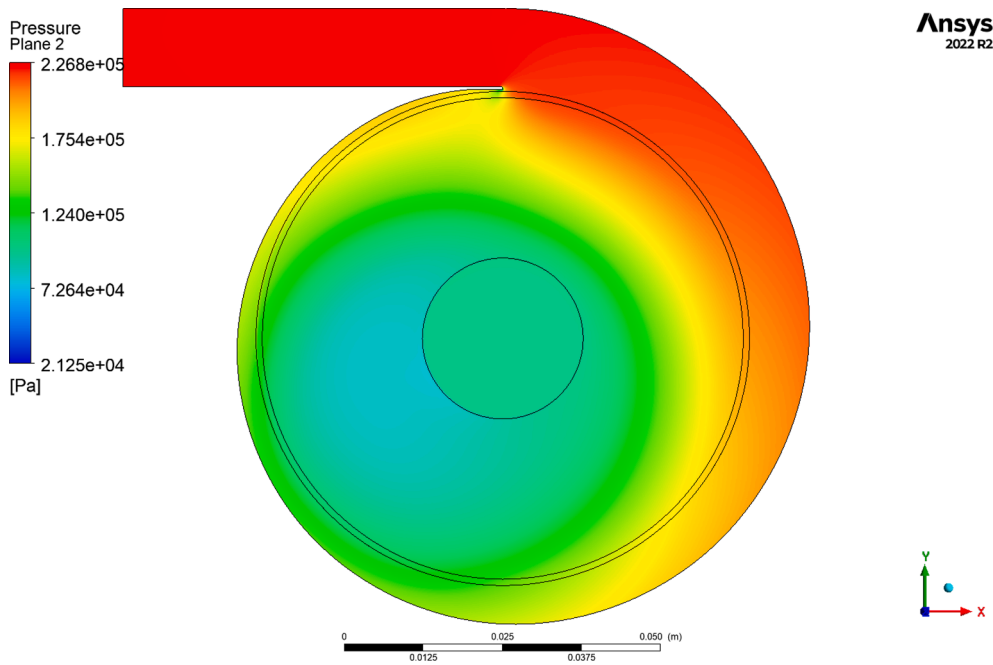
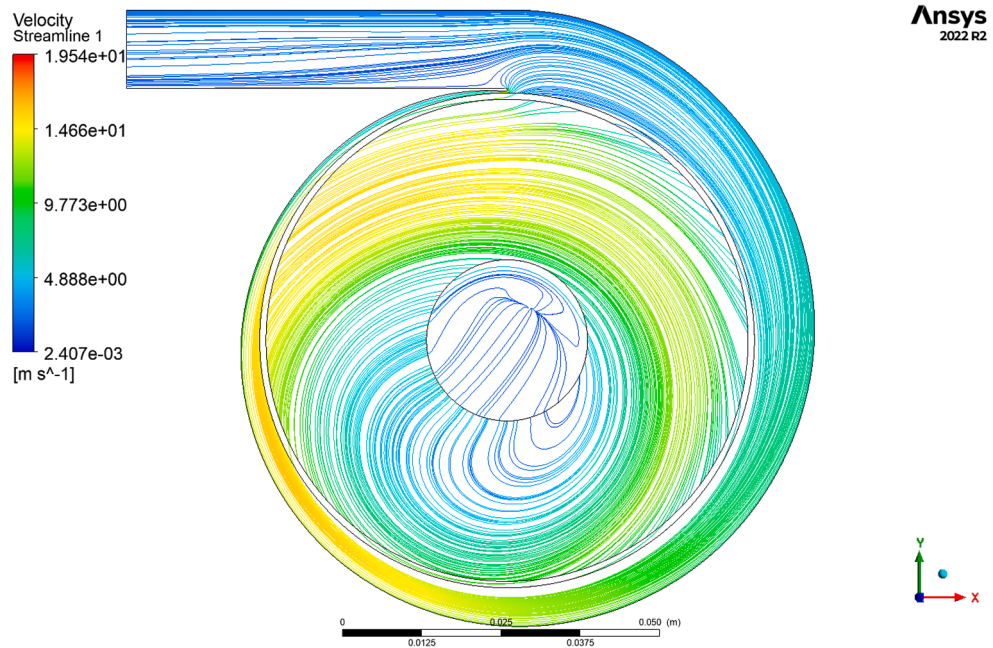**Fig. 16.** Pressure contour inside of a gap.

Fig. 17. Streamlines inside a gap.

mostly because of torque calculation are performed differently. In the CFD simulation, torque is calculated as the sum of the axial torque exerted by the fluid at every rotating surface of the discs, including the periphery at their outlet.

Comparing the 2D and CFD results at 5000 rpm, the highest efficiency with CFD is obtained at 1.94 l/s volume flowrate, differently from the initial 2D design point at 0.9 l/s. The streamlines at this rotational speed (Fig. 22) remark that there is no reverse flow, the velocity field is more symmetric, and the volute accommodates the flow better. All the above imply that to get most of the benefits of boundary layer pumps, more detailed evaluation approaches are required to capture all the flow

characteristics, which cannot be modelled with sufficient accuracy solely by a 2D code. As has been observed in literature [31] most losses occur at the interface between the rotor and volute which are best captured with 3D CFD full pump approaches since the code models the rotor and volute as black boxes and uses the solution of the rotor flow as input for the volute. Hence, it cannot capture backward effects from the volute to the rotor. An example can be seen in Fig. 23 where the vectors of radial velocities are plotted for the point 5000 rpm and 1.94 l/s on the middle meridional plane. The velocity profiles after the outlet of the rotor are different for each rotor gap because they are affected by the recirculation in the volute, contrary to the 2D approach where they are
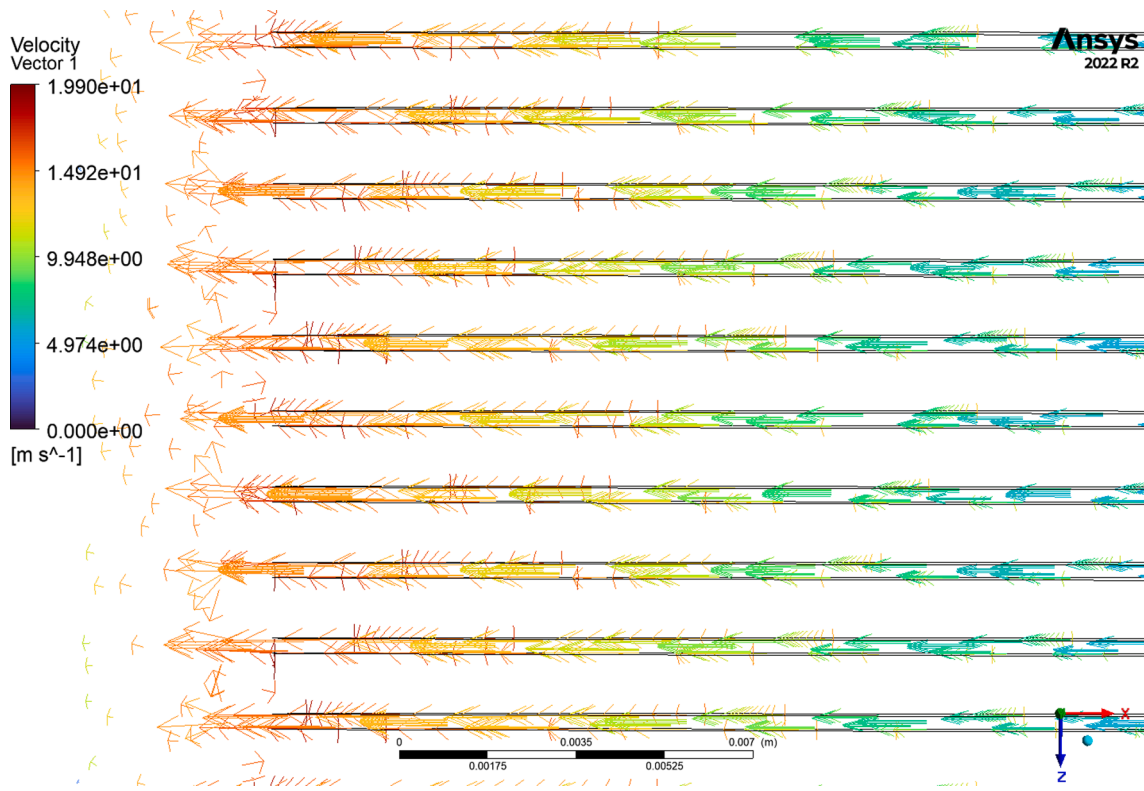
Fig. 18. Detail of the rotor outlet at the negative side of x axis where no flow reversal occurs.
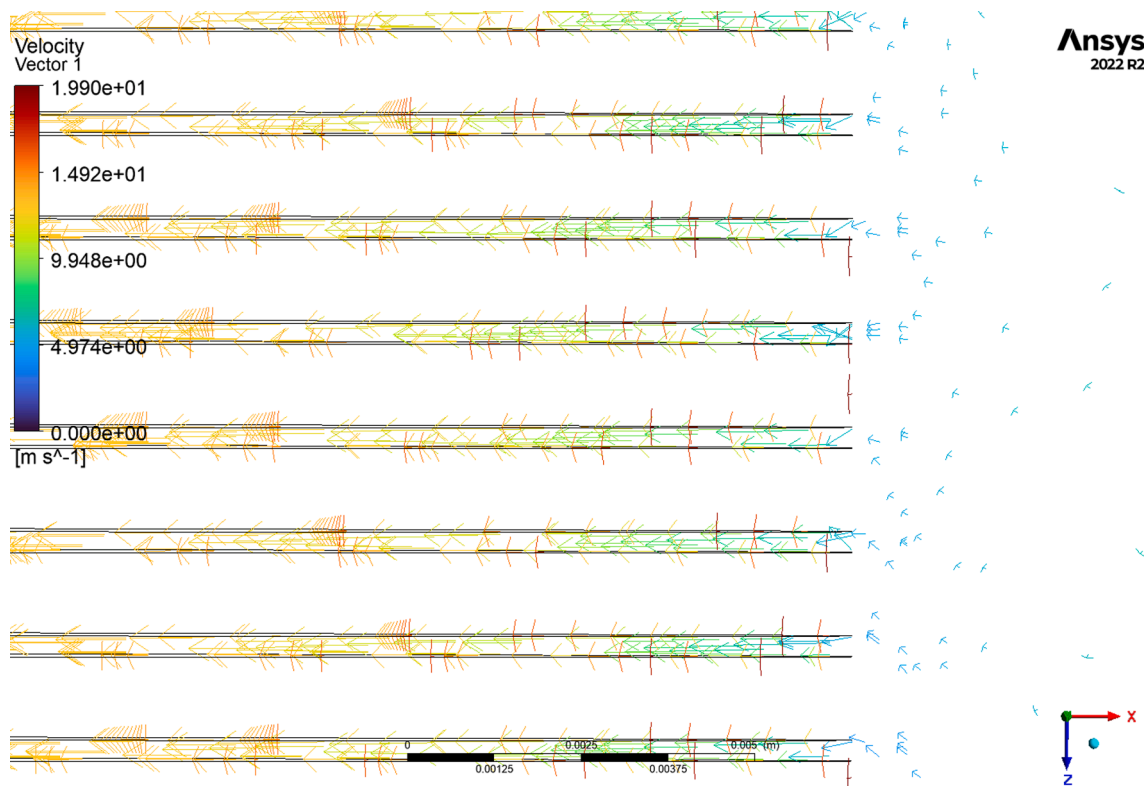
Fig. 19. Detail of the rotor outlet at the positive side of x axis where flow reversal occurs and the vectors indicate that fluid enters the rotor from the volute.

all assumed same. On the leftmost channel we even have flow reversal. All these phenomena cannot be captured by 2D approaches.

The latter remark paves the way to future investigations into volute design, and to examine the interaction between rotor and volute. However, these insights out of scope for developing a first functional prototype. It is worth to notice that the geometries investigated in the

Characteristic Curves

Fig. 20. Characteristic curves as generated by CFD and Design Code comparison.

Hydraulic Efficiencies

Fig. 21. Hydraulic Efficiencies as calculated by CFD and Design Code comparison.
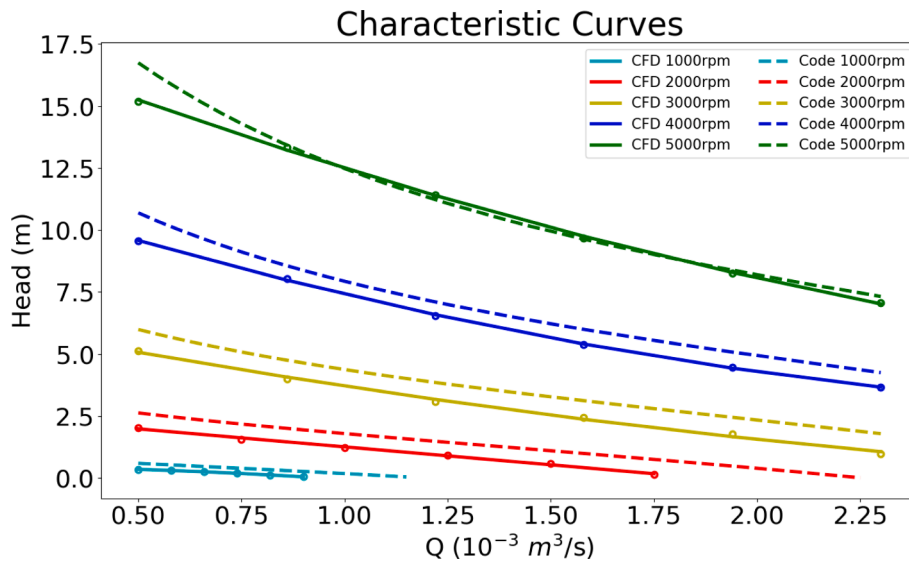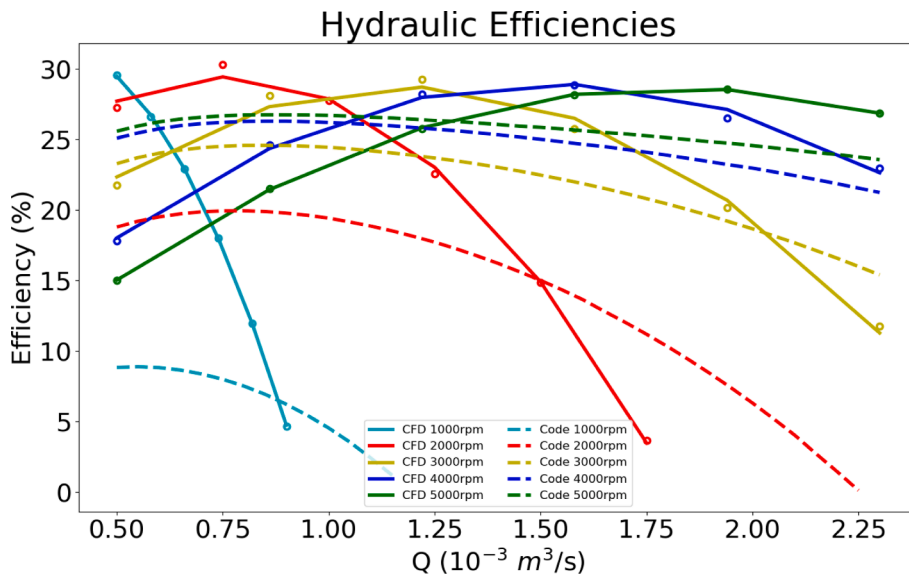
Table 5
Mean absolute error of head between the code and CFD generated curves.

	1000 rpm	2000 rpm	3000 rpm	4000 rpm	5000 rpm
Error [%]	88	43	24	10	3

CFD analysis, although near to the manufactured piece, still require further refinement. Elements such as interference from the bolts keeping together the discs, or leakages and entrained recirculating flow are not taken into consideration for this first prototype.

5. FEM analysis

FEM simulations were used as support to the mechanical design, in order to identify critical issues and fix them. Two different software (Solidworks and Ansys) were used and the related results were compared. Two types of static analyses were conducted, using a simplified rotor model: the first one considering only the gravitational force, while the second one added the centrifugal force contribution to simulate real working conditions at 5000 rpm. The in-house components were made in Aluminium. This material is cheap, easy to manufacture and prevents rust. In this project, it was assumed that standard components were realized with the same material, such as a structural steel, in order to ease the modelling process. Both of the software had a large materials database, making the selection of the proper one easy. The challenge was finding, within the database, materials closely matching the ones actually planned to be adopted, possibly being similar in the two software. This choice was done because different inputs, such as different materials, can significantly affect the final results of the mechanical analysis. In Solidworks Simulations, 1060 Aluminium Alloy was chosen for the in-house parts and AISI 304 for the standard components. In Ansys, Aluminium Alloy and Structural Steel were selected for the two parts. In the simplified model, the bearings were not taken into account; constraints were required to simulate the bearings. In Solidworks Simulations, specific constraint called "Bearing Support" was used. Self-alignment was chosen to prevent unrestricted off-axis shaft rotation. In Ansys environment, the bearings were modelled as a
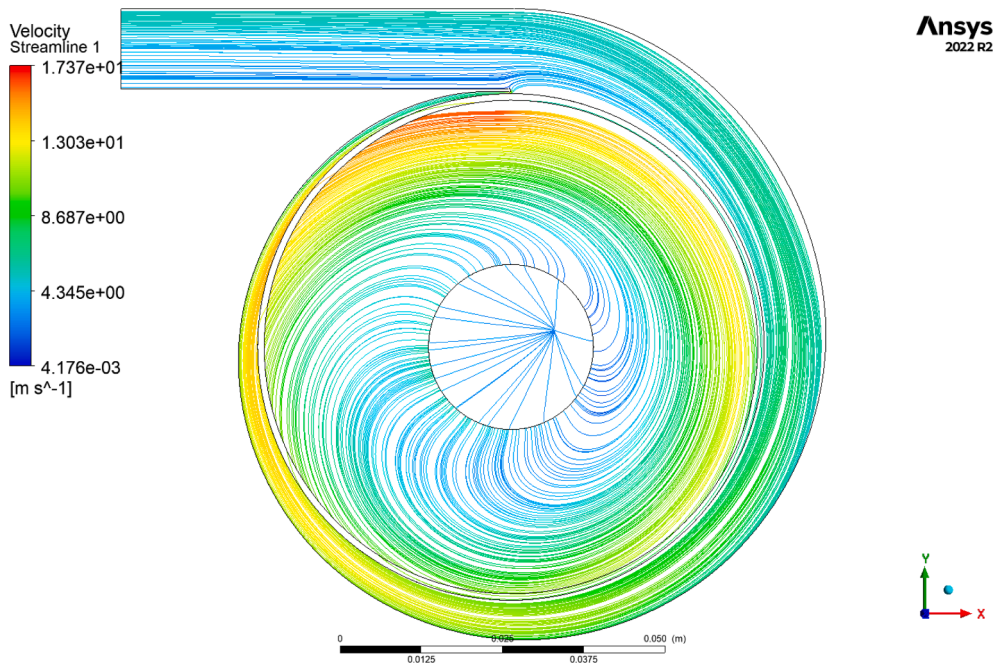
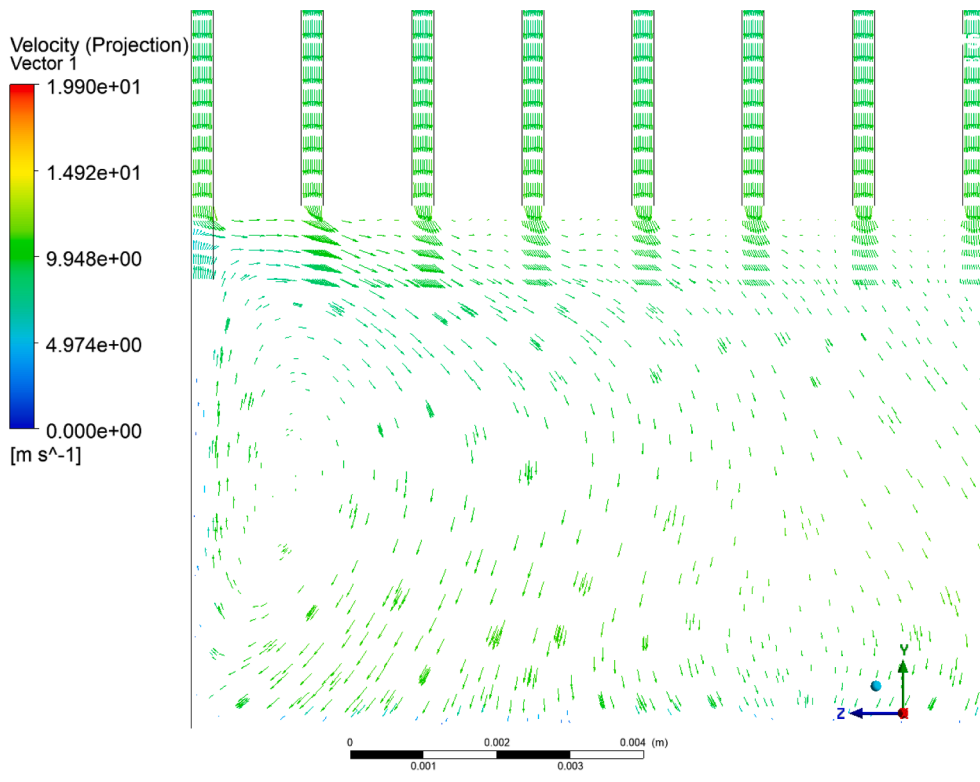**Fig. 22.** Streamlines of the 5000 rpm case with 1.94 l/s volume flow.

Fig. 23. Detail of the radial velocity vectors at the interface between rotor and volute.

cylindrical constraint with tangential displacement free to move. In this model, it was assumed that constraints are completely stiff. This assumption could be a problem and gives results far from the real conditions because actually, bearings are flexible, allowing radial and axial deformations. In FEM analysis, meshing is a critical process, which influences the accuracy of the results and the computational efficiency of the analysis. It requires a careful trade-off between accuracy and computational effort, since a finer mesh will generally provide more

accurate results but will also increase computation time. Same parameters were used for meshing process in both of the software in order to obtain similar meshes. The quality of the mesh is critical to the accuracy and reliability of simulations. In this project, quality check of the mesh was performed taking into account two parameters: Aspect Ratio and Jacobian. Both of the meshes respected the high-quality mesh standard for the software.
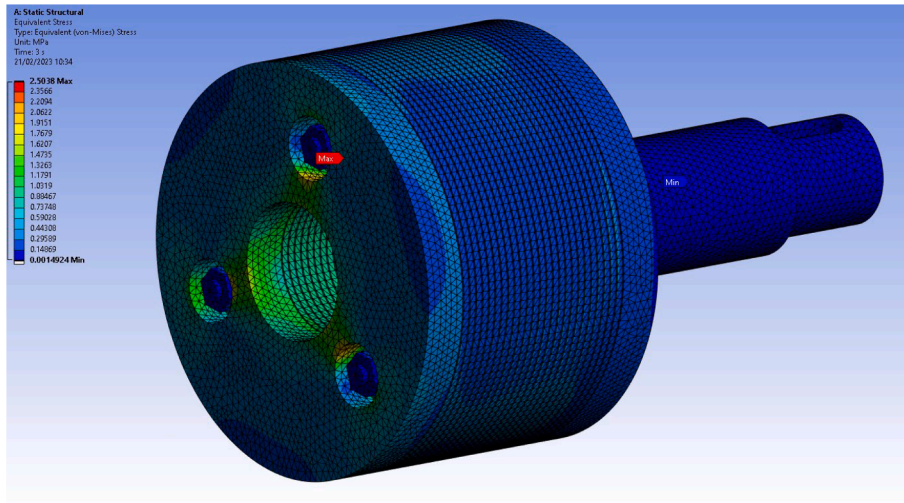
Fig. 24. Stress distribution in rotational analysis in Ansys.

5.1. Results of rotational analysis

As from the previous simulation, in both of the software, the maximum stress values resulted very similar, largely below the yield stress. From Solidworks results, the most stressed component was one of the bolts keeping discs and washers in the fixed position, with maximum value at 2.785 MPa. Ansys achieved similar results with the bolt resulting the most stressed component at the very similar value of 2.50 MPa as shown in Fig. 24. The results highlighted an interesting observation; e.g. both of the software addressed an unique maximum value of stress for one component only. With a slight deepening the analysis, it was easy to verify that the three bolts had similar stress values due to the rotational speed and centrifugal force. In both of the software, the flange resulted in the maximum strain that it could be assumed negligible
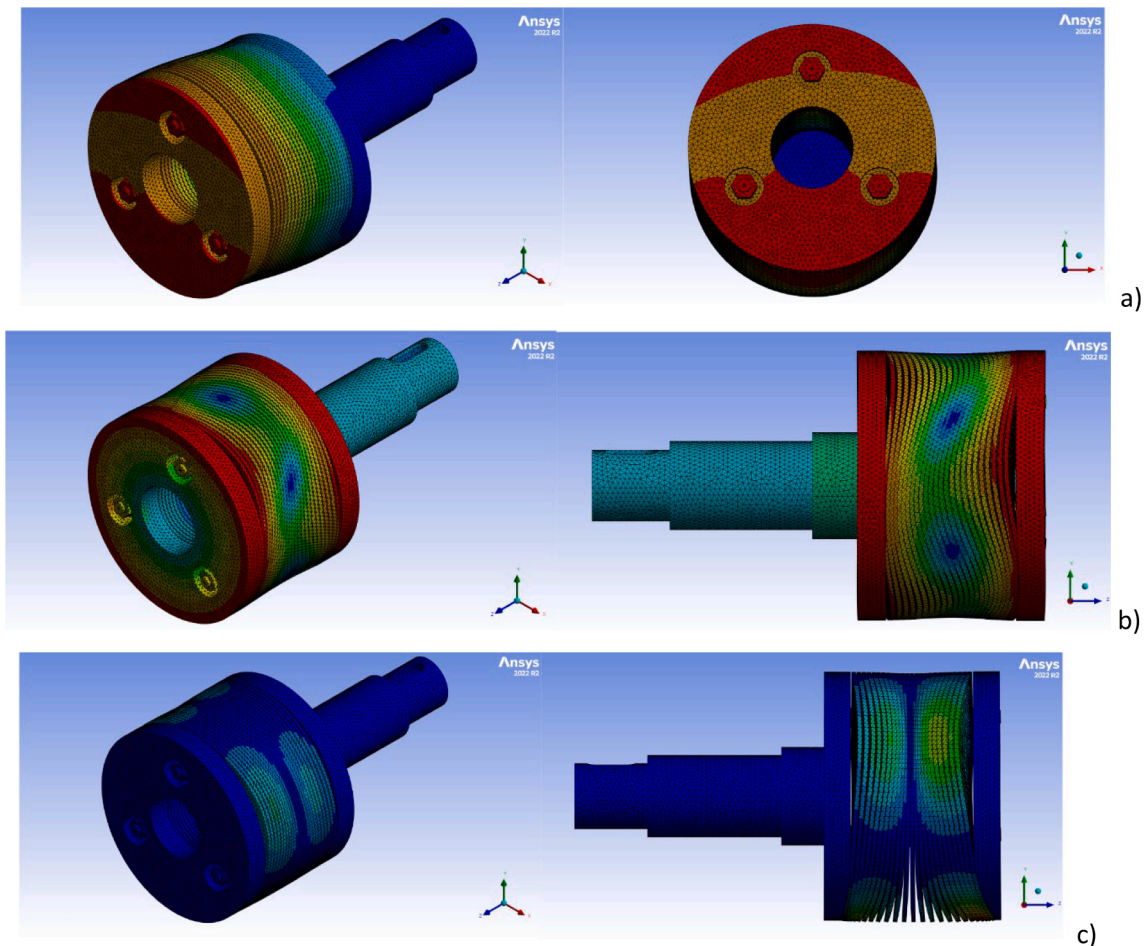

Fig. 25. Vibration modes in Ansys: a) First mode (bending category) at 678 Hz. b) Third mode (torsional category) at 1264 Hz. c) Fourth mode (disc vibration) at 1571 Hz.

because it is close to zero. These results look consistent with the real rotor working condition.

5.2. Results of modal analysis

This analysis aimed at analysing the dynamic behaviour of the rotor, with a special focus on the identification of its critical frequencies and vibration modes. To achieve this, a modal analysis was conducted using the two software, e.g. Solidworks simulation and Ansys mechanical. The required input was the number of frequencies. After running multiple simulations, twelve frequencies were selected as the optimal amount to catch the rotor's behaviour, enough to cover the real range of frequencies. A comparison of the results obtained from both of the software indicated a discrepancy less than 1 % between the corresponding values. The first critical frequency was approximately 670 Hz, this value was much higher than the maximum operating conditions of the rotor (83 Hz at 5000 rpm). This suggested that the rotor is operating in a safe zone and there is no evidence of resonance phenomena occurring. Given the complexity of these properties and factors, the analysis of each individual mode was very hard. However, a criterion to divide the modes into three categories was identified. To explore this phenomenon, several simulations were performed with different number of discs (zero, one, five, complete assembly) and the observed results appeared consistent across all the scenarios. Specifically, three categories were observed in each simulation, providing strong evidence for the criterion's validity. The first identified category was that of inflectional modes, the first and second modes of vibration were bending modes. Rotor and, specifically, flange, screws and discs pack moved on a plane perpendicular to the rotational axis. The second category consisted in a torsional vibration mode. The third mode was purely torsional, because there was a movement only around rotor rotational axis. Discs vibration represented the third and final category. Starting from the fourth mode onward, vibration modes of the rotor were a mix of modes of the single discs. While all other components remained motionless, the discs only had motions perpendicular to their plane. In Fig. 25 a, 25b and 25c, the three categories are shown. Because each disc had its own vibration mode and each rotor mode was a combination of 25-disc modes, it was impractical to conduct an in-depth analysis of every single mode of this category, as it would require a significant amount of time and computational power without giving further relevant information. It was important to investigate the underlying reasons of these behaviours. For each category, the components and their influence on the rotor vibration were thoroughly analysed. It revealed that, for the first and second category, the screws holding discs and washers in position were the main components affecting the vibration modes. A simulation of the shaft and the three screws was performed by examining the combination of the screw's free movements.

In this way, it was possible to characterize and catch the rotor vibration modes. Specifically, in the first and second mode, all three bolts moved synchronously in the same direction. The movements in the first and second mode defined the first bending category of the full rotor. Moving on the third vibration mode, the screws moved in different directions, resulting in a torsional deformation of the rotor (the second purely torsional category). Both software addressed this behaviour. From the fourth mode onward, the discs were the main components affecting the third category of vibration of the rotor. The simulation of the rotor with one disc only revealed that the single disc has only three significant vibration modes. The disc, due to the three bolts, could be divided ideally into three parts, or lobes. Each one can be moved in a specific way. Depending on how the lobes move in combination with each other, the disc will vibrate in specific modes. Three types of vibration were identified: the first one occurred when two of the three lobes moved asynchronously, while the third one remain still; the second one occurred when two lobes moved synchronously in one direction while the third one moved in the opposite direction; finally, the third one occurred when all three lobes moved together synchronously. By combining these movements for every disc, the overall set of vibration modes of the rotor can be determined.

The bearings played a crucial role in the model because, despite in most typical mechanical analyses they are assumed to be perfectly stiff, actually they are not so. The first step to analyse this occurrence consisted in a free-free modal analysis of the rotor without bearing constraints, allowing all degrees of freedom to be free. Another important modal analysis was performed by using a mathematical model to calculate a real value of the bearing stiffness. The comparison of the critical frequency's values obtained in the three types of simulations was particular interesting. Its significant impact on the first three critical frequencies became evident (bending and torsional modes), whereas the values starting above the fourth frequency were similar because the discs were the main relevant component. It was also noteworthy that the first three frequencies of the stiff bearings had higher values than those of the deformable ones. This condition was in agreement with the expected dynamic behaviour of the system. In all the three analysed cases, there was a noticeable sharing into the same categories: bending, torsional and discs vibration modes. The presence of the same pattern in all the three simulations suggests that the stiff modelling of the bearings is adequately representative of the real dynamics of the bearings, or, at least, sufficient for the purpose of this first prototype.

6. Manufacturing analysis

The manufacturing analysis influences the prototype design as provide boundaries about the features that can be achieved considering budget, in-house manufacturing capabilities, machinery and suppliers availability. It starts with the reverse engineering on existing models of Tesla pumps, and assessing which off-the-shelf components could be integrated into the design of the prototype. Here a brief list of the manufacturing analysis that influenced the prototype design:

1. Availability of prime movers and power transmission systems linked to a specific budget, determined the rotational speed of the prototype (5,000 rpm).
2. The thickness of the discs was influenced by the manufacturing and assembly methods available in-house at the time of building the prototype. Disc thicknesses between 0.127 and 0.508 mm are often quoted [4], but this range presents manufacturing challenges, considering that standard household aluminium foil is typically 0.2 mm. These challenges include maintaining roundness and flatness during cutting. Additionally, deformation of the thinner discs was observed during initial manufacturing, handling and assembly. The choice of 1.2 mm thickness for the first prototype was made to facilitate understanding of rotor assembly, with the expectation of improving this feature in the future.
3. Gap between the discs also influenced by the availability off-the-shelf washers. 0.3 mm thickness plastic washers dictated 2D and CFD analysis, but once torque is applied to the assembly, deformation occurs and even gap distribution is reduced.
4. Volute tongue gap and shape requires a few iterations between the CFD and manufacturing teams. Achieving specified optimal radius, angle of attack and intrusion length of the tongue implies relevant manufacturing CNC capabilities.
5. Maximum number of discs and therefore length of the rotor: it was influenced by the total length of aluminium block which could be outsourced to manufacture the volute in one piece. This length also influences the shape of the volute and its area distribution around the rotor. In future prototypes, the design will dictate how to manufacture the volute.

Once the prototype's sketch design was frozen, standard components were sized and selected according to standards or vendor advice. Defining tolerances was a compromise between theoretical expectations, experience and machine capabilities. Two critical parts of the
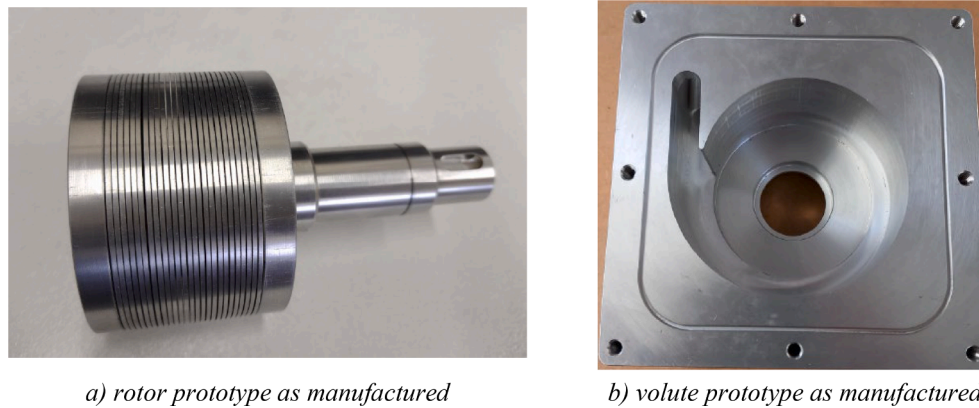
a) rotor prototype as manufactured

b) volute prototype as manufactured

Fig. 26. Volute and rotor prototype manufactured.

prototype were the water inlet and outlet. Water enters into the pump through a pipe screwed onto the casing. While this inlet solution proved to be the optimal one, it could entail reverse flow phenomena inside the pump, not reaching the rotor pack. The outlet section proved to be very complex to model, since its shape and size were fixed by the geometry and the shape of the volute. It was necessary to introduce a new part, connected with screws to the casing, allowing modification of the section from rectangular to circular through a diffuser. A pipe with the same size as the inlet was screwed onto this part.

Once the individual pieces were manufactured, challenges of assembly were addressed. Special features were design and manufactured to fit concentrically the discs and washers against the three bolt rods. The bolts needed to be seated against the socket heads shoulders and keep firm without bolting the end flange. Balancing the rotor was not possible for this first prototype but should be taken into consideration in the future. Static sealing between machined faces was achieved for the water application, however, other possible working fluids will likely require deeper research about materials to be used, temperatures ranges and general assembly.

The manufactured volute and rotor final design are shown finally in Fig. 26.

7. Conclusions

A complete design procedure for a Boundary layer pump was carried out in this work by evaluating the hydraulic performance and mechanical integrity of a boundary layer pump to operate with water. The key outcomes of the present work may be summarised as follows:

- The design of an efficient boundary layer pump rotor is achievable following 2D methods derived from an existing literature approach on Tesla turbines [21]. As previous studies indicated [35], the velocity profiles that include radius corrections perform better than typical parabolical velocity profiles, but they are not the reason to expect poor performance of the Tesla pumps.
- Running parametric studies around nondimensional parameters such as: disc diameter ratio, ratio disc thickness / disc gap; and dimensional parameters such as: rotating speed, number of discs, gap width and disc thickness; provides guidelines of optimal designs. However, these values need feedback from CFD, FEA and manufacturing analysis before being implemented.
- The basic design of the prototype has been assessed by a CFD analysis, which gives insights into the flow field and allows a more reliable evaluation of the hydraulic efficiency of the pump. The head characteristics and efficiency curves are constructed based on CFD results. The CFD results agree with the 2D method results in terms of the Head, but the pressure rise appears to be lower in the CFD results because the losses are calculated in a more accurate way. In terms of

efficiency, the 2D results do not match with the CFD ones not only because of the mismatch in total pressure rise but mostly because of the discrepancies of how to estimate torque.
- CFD analysis showed that the volute design is poor in terms of cross-sectional areas and the clearance between the rotor and volute is too small, both elements affecting the rotor flow. Therefore, the interaction between the volute and the rotor are the key elements to increase the overall efficiency of boundary layers pumps.
- This design was also assessed using FEM techniques. The presence of two critical components was confirmed: bearings and bolts. The formers introduce an uncertainty in the performance of the equipment because they are assumed as perfectly stiff in the modal analysis, a feature which in reality isn't possible. On the other hand, bolts resulted being the most stressed components, having a relevant influence on the values of natural vibration frequencies of the rotor.
- As an outcome of the developed model, a prototype was designed with water as a working fluid. The expected maximum efficiency achieved from the prototype is less than 30 % with a rotational speed of 5000 rpm and a disc gap of 0.3 mm.

As a final remark, the here conducted analysis showed how the complete assessment of a Boundary Layer or Tesla pump requires a few spirals of interactions between the hydraulic design and the manufacturing capabilities. The adopted design methodology, combining 2D basic approach and 3D refinement, and the sensitivity analysis to the most relevant parameters, show a path towards design optimization of these pumps.

Declaration of competing interest

The authors declare that they have no known competing financial interests or personal relationships that could have appeared to influence the work reported in this paper.

Data availability

Data will be made available on request.

References

[1] W. Rice, An analytical and experimental investigation of multiple-disc turbines, ASME J. Eng. Power 87 (1965) 29–36.

[2] S.H. Hasinger, L.G. Kehrt, Investigation of a Shear-Force Pump, ASME Trans. J. Eng. Power 85 (3) (1963).

[3] O.E. Balje, Turbomachines. A guide to design, selection and theory, 1981. https://doi.org/10.1115/1.3241788.

[4] J.H. Morris, Performance of Multiple-Disc-Rotor Pumps with varied interdisc spacings, David W. Taylor Naval Ship R and DCenter Bethesda, MD, U.S. Navy Report Number DTNSRDC-80/008, August 1980.

[5] J. Pacello, P. Hanas, Disc pump-type pump technology for hard-to-pump applications, Proceedings of the 17th international pump users symposium, Texas, 2000.

[6] N. Tesla, "Turbine", U.S. Patent No. 1 061 206, 1913.

[7] A.B. Leaman, The design, construction and investigation of a Tesla turbine, M.S. Thesis, University of Maryland, 1950.

[8] J.H. Armstrong, An Investigation of the Performance of a Modified Tesla Turbine, M.S. Thesis, Georgia Institute of Technology, 1952.

[9] E.W. Beans, Performance characteristics of a Friction Disc Turbine, PhD Thesis, Pennsylvania State University, 1961.

[10] L. Matsch, W. Rice, Flow at low Reynolds number with partial admission between rotating discs, in: Transactions of the ASME, Journal of Applied Mechanics, 1967.

[11] W. Rice, An analytical and experimental investigation of multiple disc pumps and compressors, J. Eng. Power 85 (3) (1965) 191–198.

[12] K.E. Boyd, W. Rice, Laminar inward flow of an incompressible fluid between rotating discs, with full peripheral admission, J. Appl. Mech. (1968) 229–237.

[13] L. Matsch, W. Rice, Potential flow between two parallel circular discs with partial admission, in: Transactions of the ASME, Journal of Applied Mechanics, 1967.

[14] L. Matsch, W. Rice, An asymptotic solution for laminar flow of an incompressible fluid between rotating discs, in: Transactions of the ASME, Journal of Applied Mechanics, 1968.

[15] W. Rice, An analytical and experimental investigation of multiple-disc turbines, J. Eng. Gas Turbines Power 87 (1) (1965), https://doi.org/10.1115/1.3678134.

[16] P.J. Roddy, Ron Darby, G.L. Morrison, P.E. Jenkins, Performance Characteristics of a Multiple-Disc Centrifugal Pump, J. Fluids Eng. 109 (1) (1987), https://doi.org/10.1115/1.3242616.

[17] M. Foster, The potential of a Tesla type device as a non pulsatile blood pump, Middlesex University of London, 2006.

[18] P. Bloudicek, D. Palousek, Design of Tesla Turbine, in: Proceedings of Konference diplomovych praci, Brno, 2007.

[19] B. Wang, K. Okamoto, K. Yamaguchi, S. Teramoto, Loss mechanisms in shear-force pump with multiple corotating discs, J. Fluids Eng., Trans. ASME 136 (8) (2014), https://doi.org/10.1115/1.4026585.

[20] L. Dodsworth, D. Groulx, Operational Parametric Study of a Tesla Pump: Disc Pack Spacing and Rotational Speed, 2015. https://doi.org/10.1115/ajkfluids2015-33220.

[21] L. Talluri, O. Dumont, G. Manfrida, V. Lemort, D. Fiaschi, Geometry definition and performance assessment of Tesla turbines for ORC, Energy 211 (2020) 118570.

[22] L. Martínez-Díaz, H.H. Herrera, L.M.C. González, N.V. Izquierdo, T.R. Carvajal, Effects of turbulization on the disc pump performance, Alex. Eng. J. 58 (3) (2019), https://doi.org/10.1016/j.aej.2019.03.011.

[23] Eduardo Anselmi Palma; Daniele Fiaschi; Giampaolo Manfrida; Giovanni Nicotra; Lorenzo Talluri, Design and optimization of a Tesla pump for ORC applications, Proceedings of the 6th International Seminar on ORC Power Systems, October 11-13, 2021, Munich.

[24] D.H. Alonso, L.F. Nogueira de Sà, J.S.R. Saen, E.C.N. Silva, Topology optimization based on a two-dimensional swirl flow model of Tesla-type pump devices, Comput. Math. Appl. 77 (2019) 2499–2533.

[25] Y. Heng, Y. Han, H. Zhang, W. Zhang, G. Bois, Q. Jiang, Z. Wang, X. Liu, Tesla bladed pump (Disc Bladed Pump) preliminary experimental performance analysis, Energies 13 (18) (2020), https://doi.org/10.3390/en13184873.

[26] A. Renuke, A. Vannoni, M. Pascenti, A. Traverso, Experimental and numerical investigation of small-scale tesla turbines, J. Eng. Gas Turbines Power 141 (12) (2019) 4044999, https://doi.org/10.1115/1.4044999.

[27] A. Renuke, F. Reggio, A. Traverso, M. Pascenti, Experimental Characterization of Losses in Bladeless Turbine Prototype, J. Eng. Gas Turbines Power 144 (4) (2022) 041009, https://doi.org/10.1115/1.4053117.

[28] S. Sengupta, A. Guha, A theory of Tesla disc turbines, Proceedings of the Institution of Mechanical Engineers, Part A: Journal of Power and Energy 226 (5) (2012) 650–663.

[29] R.D. Braembussche, Flow and loss mechanisms in volutes of centrifugal pumps, Design and analysis of high speed pumps (2006) 1–26.

[30] L. Dodsworth, Operational Parametric Study of a Prototype Tesla Pump, Dalhousie University, Halifax, Nova Scotia, 2016.

[31] K. Palaveev, D.J. Rajendran, E. Anselmi, M. Santhanakrishnan, V. Pachidis, Insights Into The Flow Field And Performance Of A Boundary Layer Pump, Proc. ASME Turbo Expo 9 (2023), https://doi.org/10.1115/GT2023-102186.

[32] Thermodynamic and Transport Properties Database (REFPROP): Version 10, NIST v 10.0, Nist Standard Reference Database 23 DLL version number 10.0.

[33] S.M. Salim, S.C. Cheah, Wall y+ strategy for dealing with wall-bounded turbulent flows, Int. Multiconf. Eng. Comput. Sci. (IMECS) 2 (2009) 1–6.

[34] I.B. Celik, U. Ghia, P.J. Roache, C.J. Freitas, H. Coleman, P.E. Raad, Procedure for Estimation and Reporting of Uncertainty Due to Discretization in CFD Applications, J. Fluids Eng. 130 (7) (2008), https://doi.org/10.1115/1.2960953.

[35] R. Freschi, A. Bakogianni, D.J. Rajendran, E.A. Palma, L. Talluri, I. Roumeliotis, Flow Field Explorations in a Boundary Layer Pump Rotor for Improving 1D Design Codes, Designs 7 (1) (2023), https://doi.org/10.3390/designs7010029.